nature chemistry

ARTICLES

PUBLISHED ONLINE: 20 NOVEMBER 2017 | DOI: 10.1038/NCHEM.2889

Structure-based inhibitors of tau aggregation

P. M. Seidler[1,2], D. R. Boyer[1,2], J. A. Rodriguez[1,2], M. R. Sawaya[1,2], D. Cascio[1,2], K. Murray[1,2], T. Gonen[3] and D. S. Eisenberg[1,2]*

Aggregated tau protein is associated with over 20 neurological disorders, which include Alzheimer's disease. Previous work has shown that tau's sequence segments VQIINK and VQIVYK drive its aggregation, but inhibitors based on the structure of the VQIVYK segment only partially inhibit full-length tau aggregation and are ineffective at inhibiting seeding by full-length fibrils. Here we show that the VQIINK segment is the more powerful driver of tau aggregation. Two structures of this segment determined by the cryo-electron microscopy method micro-electron diffraction explain its dominant influence on tau aggregation. Of practical significance, the structures lead to the design of inhibitors that not only inhibit tau aggregation but also inhibit the ability of exogenous full-length tau fibrils to seed intracellular tau in HEK293 biosensor cells into amyloid. We also raise the possibility that the two VQIINK structures represent amyloid polymorphs of tau that may account for a subset of prion-like strains of tau.

The 441-residue protein tau is abundant in neurons where, in its native state, it is bound to microtubules. In solution, tau is largely unfolded[1,2], and in the numerous neuropathologies known as tauopathies, tau is aggregated into amyloid fibrils[3]. The most-prevalent tauopathy is Alzheimer's disease (AD), in which aggregated tau is found as intracellular 'tangles' first reported by Alzheimer. Until recently, tangles were observed only in stained brain sections on autopsy. The development of positron-emission tomography probes is helping to illuminate the course of AD progression, and it is becoming evident that cognitive decline in AD is tightly coupled to the appearance of tau aggregates in the brain[4]. Furthermore, evidence suggests that amyloid β-plaques can form early on and may set the stage for tau aggregation and disease progression[5–7]. Once formed, tau pathology is thought to spread along connected neuronal networks in the brain by transcellular propagation of aggregated tau[8].

In normal neurons, tau promotes microtubule stability by binding tubulin through its microtubule binding domain (K18) that comprises four imperfect repeats. Six tau isoforms encode variable architectures, the longest of which contains all four repeats (4R), whereas a shorter isoform with three repeats (3R) lacks repeat 2 (R2). Driving the formation of amyloid aggregates of tau are two six-residue segments, VQIINK at the start of R2 and VQIVYK at the start of repeat 3 (R3) (Fig. 1a)[2,9].

Highly specific inhibitors of tau aggregation are needed to determine definitively if and how tau aggregates lead to cognitive decline in AD and other tauopathies. Furthermore, inhibitors that block seeding by capping the ends of tau fibrils could halt the progression of tau pathology in the brain. The atomic structure of an amyloid fibril formed by VQIVYK from R3 was determined in 2007[10] and the structure was used to design inhibitors of VQIVYK aggregation[11,12]. These studies demonstrated that VQIVYK inhibitors are highly effective at blocking the aggregation of 3R tau isoforms *in vitro*, but as we show here are ineffective at inhibiting the full-length tau protein (tau40), which additionally contains the VQIINK segment of R2. This observation motivated us to determine the structure of the VQIINK steric zipper.

Extending over a decade in our lab, efforts to grow crystals of amyloid fibrils of VQIINK produced only nanocrystals, far too small for single-crystal X-ray diffraction. Fortunately, with the recent advent of micro-electron diffraction (MicroED)[13–15], we have been able to determine the structures of fibrils that contain VQIINK by electron diffraction, which we report here. These structures provide the first glimpse of the VQIINK aggregation interface. Extrapolating from these structures allowed us to design VQIINK inhibitors that block full-length tau aggregation and seeding. With these and VQIVYK inhibitors in hand, we tested tau40 fibrils to determine how each of the respective segments contributes to the spread of tau aggregation by the seeding. Together, our seeding, biochemical and structural studies suggest that VQIINK is a potent driver of aggregation and seeding, and a superior target for inhibitors of tau40. Additionally, our structures offer insights into tau fibril polymorphism, which we speculate could relate to the phenomenon of tau strains.

Results

VQIINK forms an extensive steric zipper interface. To understand the forces that drive the aggregation of tau and to enable the design of inhibitors of the aggregation of tau40, we crystallized a ten-residue tau segment with the sequence KVQIINKKLD and determined its 1.5 Å resolution structure by MicroED. As for VQIVYK, this VQIINK-containing segment forms a face-to-face Type 1 homosteric zipper. That is, the protofilament is formed from the tight mating of identical parallel β-sheets, which are antiparallel to each other[16]. The VQIINK zipper shows a tighter side-chain interdigitation than the VQIVYK zipper (Fig. 1b), with a shape complementarity (S_c) of 0.77 compared with 0.72 for VQIVYK. Additionally, VQIINK buries a greater surface area, 168 Å^2, compared with 75 Å^2 for VQIVYK. These measures of the strength of interfaces suggest that the zipper interface of VQIINK is stronger than the VQIVYK interface.

Interface B. The ten-residue VQIINK segment revealed an unanticipated propensity to adopt a second steric zipper interface. The second zipper (referred to as interface B) is formed by the C-terminal half of the segment, residues KKLD (Fig. 1c). A sequence alignment that compares R2 and R3 shows that the equivalent residues in R3 are KPVD, which is not expected to

[1]Departments of Chemistry and Biochemistry and Biological Chemistry, UCLA-DOE Institute, UCLA, Los Angeles, California 90095, USA. [2]Howard Hughes Medical Institute, UCLA, Los Angeles, California 90095, USA. [3]Howard Hughes Medical Institute, Janelia Research Campus, 19700 Helix Drive, Ashburn, Virginia 20147, USA. *e-mail: david@mbi.ucla.edu

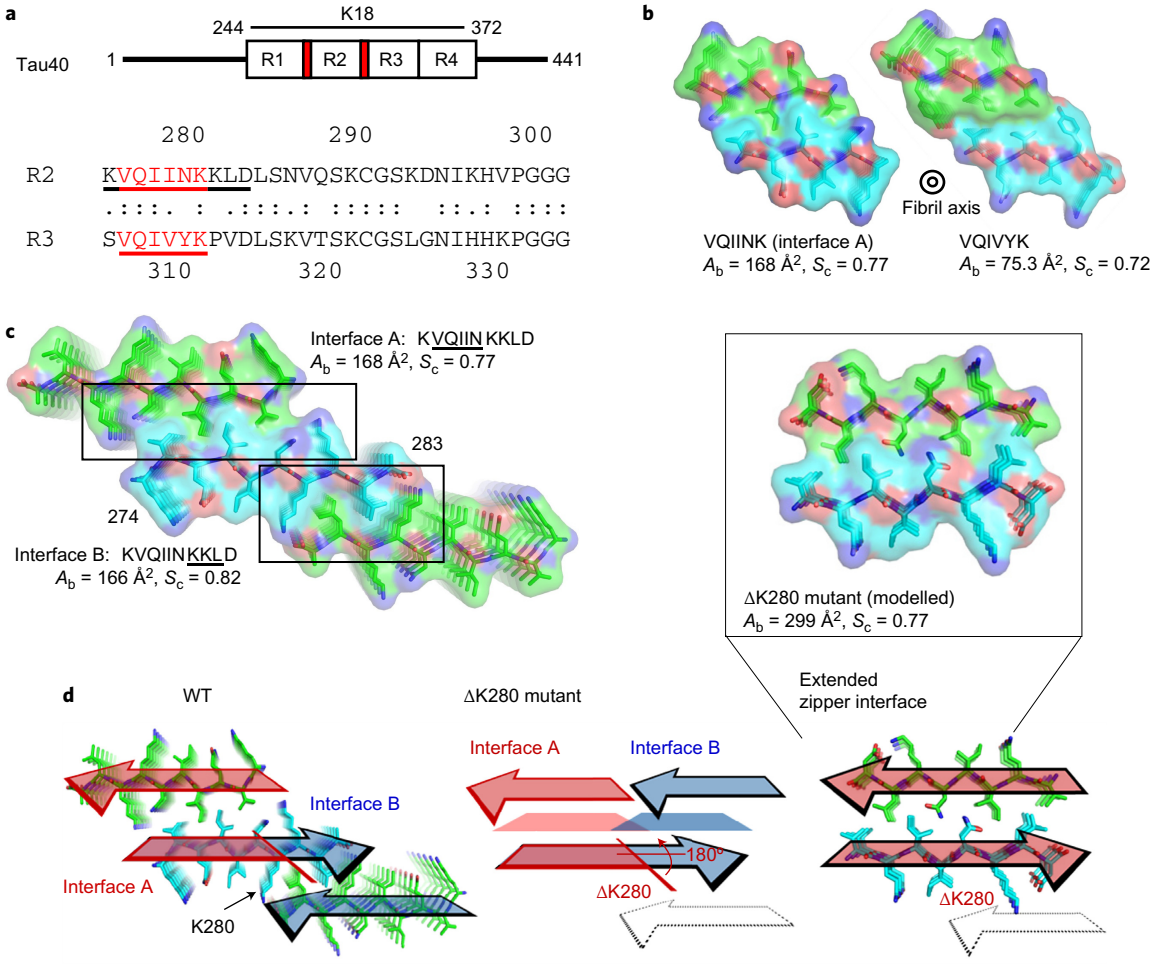

Figure 1 | Atomic structures of amyloid fibrils formed by segments of tau, viewed down the fibril axes. a, Schematic of full-length tau showing the positions of VQIINK and VQIVYK (coloured red) in the microtubule binding domain that contains four repeats (R1–R4), together termed K18. Shown below is a sequence alignment of R2 and R3 from human tau with the VQIINK and VQIVYK segments underlined. **b**, Comparison of A_b and S_c for the VQIINK (interface A (this paper)) and VQIVYK (ref. 10, PDB 2ON9) steric zippers. **c**, The two steric zipper interfaces, A and B, in the ten-residue KVQIINKKLD crystal, shown as stick models with superimposed van der Waals atomic radii. The two interfaces have similar A_b and S_c. The numbering corresponds to the N- and C-termini for the β-sheet coloured in cyan. **d**, Arrangement of interfaces A and B in the ten-residue WT KVQIINKKLD structure (left) and the predicted arrangement in the ΔK280 mutant (centre and right). Trapezoids in the centre diagram represent steric zipper-forming residues that are predicted to line the interface between the mated β-strands. The coloured arrows show the directions of the β-strands that form the steric zippers. Red, oxygen; blue, nitrogen; green, main chain for A and C; cyan, main chain for B. In the WT structure, interfaces A (red) and B (blue) are formed on opposite faces of the VQIINK β-sheet. Deletion of residue K280 is predicted to reverse the orientation of the C-terminal residues by 180° about the β-strand axes (centre) to merge steric zipper interfaces A and B into a single extended steric zipper interface with greater A_b and S_c as calculated from the ΔK280 model (right and inset).

adopt a comparable zipper because proline residues have a strong tendency to disrupt β-sheets and break amyloid structures[17] (Fig. 1a). Furthermore, an overlapping segment with the sequence LDLSN in R2, which corresponds to amino acids 282–286, bears the features of an amphiphilic amyloidogenic sequence motif, whereas no additional sequences with these features are found in R3 (ref. 18). This suggests that the potential to form a second extended steric zipper interface is limited to the R2 segment, VQIINK.

Δk280 mutant. In the wild-type (WT) segment structure, interfaces A and B are formed on opposite faces of the VQIINK β-sheet. It is known that the ΔK280 mutation accelerates tau fibre formation and has been linked to tauopathies[1,19]. Lys280 lies at the junction between interfaces A and B in our crystal structure (Fig. 1c,d) and deleting K280 is expected to reverse the orientation of the C-terminal residues by 180° about the β-strand axis[20]. The result is to rotate the zipper-forming residues in interface B to the same face of the β-sheet as interface A, merging the two separate interfaces that lie on opposite faces in the WT to a single extended zipper interface in the ΔK280 mutant (Fig. 1d, inset). Modelling the steric zipper formed by the ΔK280 mutant shows that the extended interface formed by these predicted structural changes results in a longer zipper with a high S_c (0.77) and nearly double the solvent-accessible surface area buried (A_b = 299 Å^2), which explains how the ΔK280 mutant could promote a more-rapid tau aggregation and toxicity.

VQIINK promotes rapid fibre formation. Given the observation that VQIINK forms a more-extensive steric zipper interface than VQIVYK, we wondered if VQIINK would be a more-potent driver of amyloid formation than VQIVYK. To test the possibility, we replaced the residues VY in VQIVYK with IN, which converts tau K18 into an engineered form that contains two copies of VQIINK (named 2xIN). Similarly, 2xVY was constructed and compared with WT K18 to determine how the

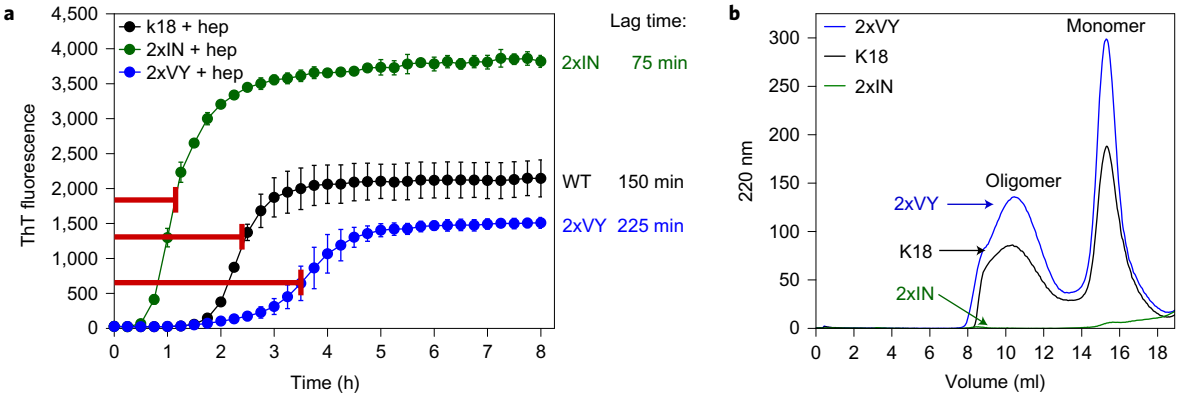

Figure 2 | Time dependence of fibrillization and oligomerization for the WT K18 construct and the 2xIN and 2xVY K18 mutant constructs. a, Averaged ThT fluorescence curves of the WT K18 construct and engineered 2xIN and 2xVY K18 constructs at 50 μM in the presence of heparin with shaking at 700 r.p.m. at 37 °C. Lag times determined from the half-maximum values of the curves shown are given for the respective constructs on the right. Error bars show the s.d. of triplicate ThT measurements. **b**, Analysis of oligomers measured by S200 size-exclusion chromatography. Peaks that correspond to the soluble oligomer species are marked with arrows.

rates of fibril formation differ for constructs that contain only VQIINK or VQIVYK zipper segments. As shown by thioflavin T (ThT) fluorescence in Fig. 2a, 2xIN exhibits a greater rate of aggregation by shaking at 37 °C with heparin, forming fibrils in half the time of WT (75 minutes versus 150 minutes to reach half maximum). 2xVY aggregates the most slowly, reaching half maximum after 225 minutes.

To evaluate how the VQIINK and VQIVIYK segments affect the formation of soluble oligomers, tau oligomers were fractionated by gel filtration chromatography. This approach has been used for K18 to separate monomer, oligomer and fibrillar species[21]. WT K18 forms a mixture of aggregates overnight, amyloid fibres and insoluble material are removed by ultracentrifugation and the resulting supernatant injected into a S200 size-exclusion column separates into two peaks, one of which contains monomer, and the other oligomer (Fig. 2b, black line). 2xVY produces a mixture of species similar to WT, whereas no remaining monomer or oligomer is detectable for 2xIN (Fig. 2b, blue and green lines, respectively). Together, these data suggest that 2xIN rapidly fibrillizes in the presence of heparin, which shifts the equilibrium away from monomeric and oligomeric species and instead favours a rapid amyloid fibre formation.

VQIINK inhibitors reduce tau fibril formation and block seeding. The VQIINK crystal structure was used as a template for a structure-based inhibitor design (Fig. 3a). The native ten-residue sequence that we crystallized was used as a starting point, and bulky amino acid side chains were modelled into the zipper to identify residues that would best disrupt the observed interfaces. As summarized in Table 1, an Ile at position 4 and a Leu at position 9 (which correspond to residues I277 and L282 in the tau40 protein sequence) were identified as key residues in interfaces A and B. Modelling indicated that interface A would be best disrupted by replacing the Ile at position 4 with either a Met or Trp, whereas interface B appeared to be best disrupted by Arg. As the native peptide sequence targeted by the inhibitor is dipolar (begins with a Lys and ends with an Asp), the terminal residues of the inhibitor peptide were charge reversed to promote electrostatic attraction with the binding interface.

The effects on the fibril formation of tau40 of the two resulting VQIINK inhibitors, MINK (which contains a Met at position 4 to disrupt interface A) and WINK (which instead contains a Trp), were evaluated *in vitro* using a ThT assay. At 25 μM tau40, a twofold mole excess of either MINK or WINK reduced tau40 aggregation to about half, with MINK inhibiting the tau40 aggregation slightly more effectively than WINK (Fig. 3b). We wondered if the MINK and WINK peptides themselves were capable of aggregating because they derive from the aggregation-prone VQIINK segment. To test the aggregation of these inhibitors, we subjected MINK and WINK to the same conditions used to aggregate tau40, that is by incubating at 37 °C with heparin and shaking at 700 revolutions per minute (r.p.m.). As shown in Supplementary Fig. 2a, WINK had no detectable aggregation, although MINK produced a low ThT signal after 24 hours that indicated some degree of aggregation. By comparison, we estimate the level of MINK aggregation to be nearly 20 times less than that of tau40.

Recent evidence suggests that aggregated tau can spread from cell to cell in a prion-like manner, apparently by seeding tau in the recipient cell into fibrils[8]. To test whether the VQIINK inhibitors are capable of blocking the spread of tau fibres by seeding, tau40 monomer was incubated at 37 °C and shaken with heparin in the presence or absence of MINK or WINK before seeding HEK293 biosensor cells that stably express a near full-length isoform, tau 4R1N P301S-EYFP[22]. As shown in Fig. 3c, about 61% of the cells that were seeded with 125 nM unlabelled tau40 fibre in the absence of inhibitor produced intracellular aggregates. Cells seeded with tau40 fibre grown with MINK or WINK reduced the percentage of seeded cells to 23 and 41%, respectively. Qualitatively, these VQIINK inhibitors improved the appearance of cells and resulted in a more typical monolayer growth rather than a rounded morphology (Fig. 3c).

To test whether VQIINK inhibitors can cap pre-formed fibres to block their spread, tau40 amyloid fibrils were incubated with varying concentrations of inhibitor before the pre-capped fibres were applied to 4R1N tau biosensor cells and the seeding measured. As shown in Fig. 3d,e, MINK and WINK inhibit seeding by tau40 fibres in a concentration-dependent fashion. From the dose–response plots shown, half-maximum inhibitory concentration (IC_{50}) values of 22.6 and 28.9 μM were calculated for MINK and WINK. In contrast, the potent VQIVYK capping peptide inhibitor with sequence TLKIVW[11] poorly inhibited seeding by tau40 fibrils (Fig. 3f). Furthermore, a combination of MINK and TLKIVW inhibitors failed to synergize, although the pair performed better than TLKIVW alone, having an IC_{50} value of 52.2 μM (Fig. 3g).

Design of Phase 2 inhibitors based on a second polymorph. We sought and discovered a second structural polymorph of amyloid fibrils formed by the VQIINK segment. Our rationale was the report that distinct strains of HEK biosensor cells are apparently caused by seeding with distinct aggregated forms of tau[22], and that K18, which contains VQIINK in addition to VQIVYK,

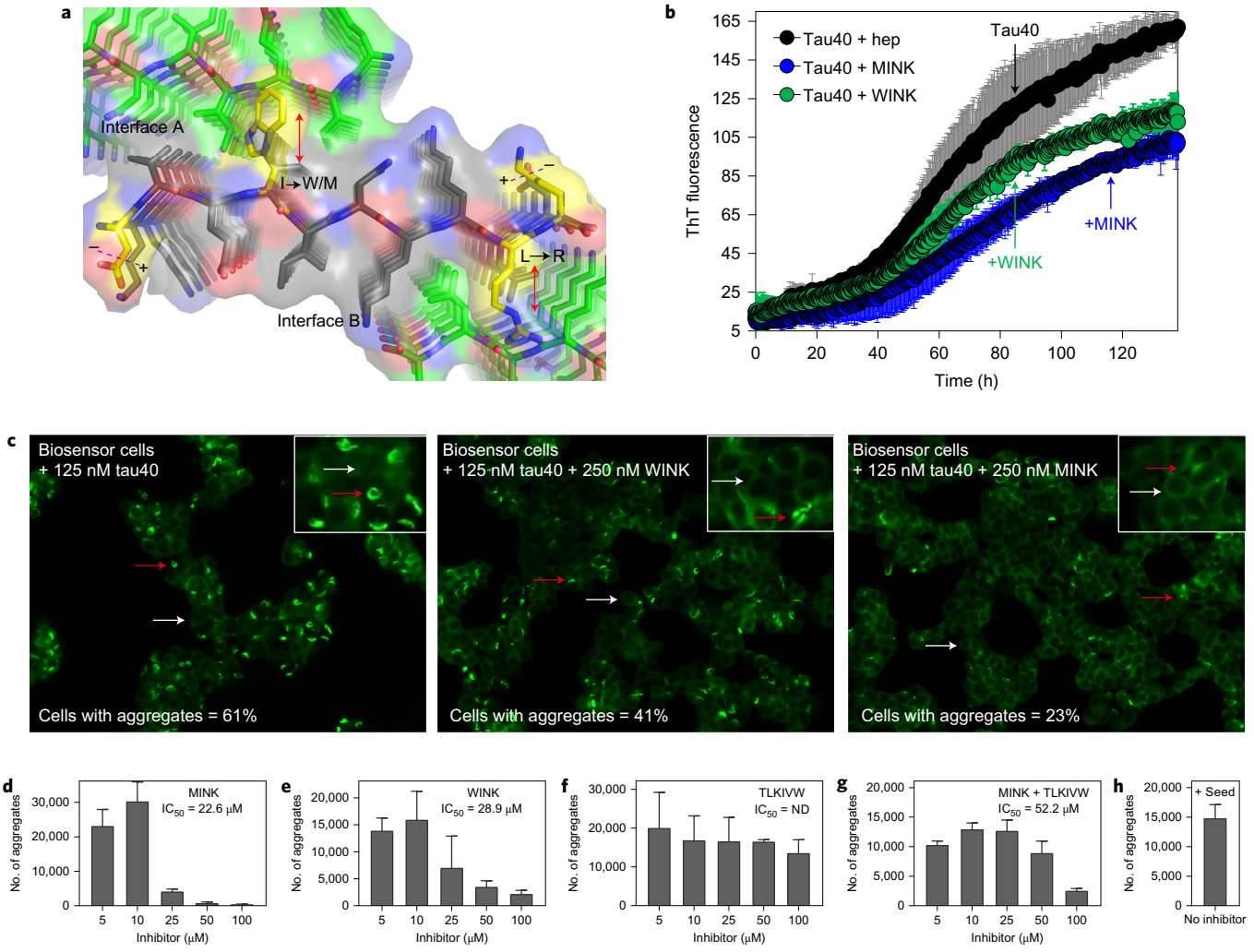

Figure 3 | Structure-based design of Phase 1 inhibitors of VQIINK aggregation. a, Logic of inhibitor design. The inhibitors (Table 1) bind on the tips of VQIINK fibrils and introduce steric clashes that disrupt interfaces A and B. Based on the structures, the inhibitor peptides deriving from the WT sequence were designed as follows. The Ile at position 4 of the peptide was replaced with either a tryptophan (inhibitor WINK) or methionine (inhibitor MINK) to block interface A (I → W/M). Both inhibitors contain a L → R substitution at position 9 to disrupt interface B. The ends of the inhibitor were charge reversed to promote electrostatic attraction of the inhibitor peptide to the fibril sequence. **b**, The effects of designed inhibitors on the formation of fibrils of 25 μM tau40 plus a twofold molar excess of the MINK or WINK inhibitor peptide with shaking at 700 r.p.m. at 37 °C. Error bars show the s.d. of triplicate ThT measurements from two independent experiments. **c**, The effects of the designed inhibitors on the transfer of fibrils of tau40 into the HEK293 biosensor that stably expresses a full-length (4R1N P301S) yellow fluorescent protein (YFP) fusion. The cells (shown at ×10 magnification) were seeded with 125 nM tau40 fibre (final concentration); the seeds were grown for 120 h in the presence or absence of a twofold excess of WINK or MINK. Representative cells that contain aggregates are marked by red arrows, and cells without by white arrows. Percentages of cells with aggregates were calculated by dividing the number of aggregates in the field of view by the number of cells. Inset boxes show magnified images (×20 magnification) from within the presented field of view. **d**–**h**, 4R1N tau–YFP biosensor cells seeded with pre-capped tau40 fibres treated with MINK (**d**), WINK (**e**), TLKIVW (**f**) or MINK + TLKIVW (**g**) inhibitor peptides at the indicated concentrations, and the effect of no inhibitor (**h**). Bar graphs show the average number of aggregates at the indicated inhibitor concentrations, and error bars show the s.d. of triplicate measurements. IC_{50} values were calculated from the dose-response plots shown. Panels **b**–**d** suggest that MINK is a more effective inhibitor than WINK.

exhibits conformational heterogeneity, whereas K19, which contains only VQIYVK, does not[23]. We screened for and found nanocrystals of the VQIINK segment and were able to determine their atomic structure by MicroED. This structure reveals a Class 4, face-to-back steric zipper, driven by Gln and Ile side chains on the opposite face of the VQIINK β-strand. We term this interface C (Fig. 4b). Interface C buries a substantial surface area ($A_b = 146$ Å^2), albeit marginally lower than that by interface A, and its $S_c = 0.67$. Apparently, the VQIINK segment of tau is capable of forming at least three distinct steric zipper interactions, which leads to at least three distinct amyloid fibrils and potentially three distinct phenotypic downstream effects.

We hypothesize that the interfaces observed in our two crystal structures represent the actual surfaces used by tau40 to form different aggregate subpopulations. To test this, we re-engineered MINK to incorporate a third steric clash that would disrupt interface C in addition to interfaces A and B. We reasoned that if multiple subpopulations of aggregates can simultaneously exist as a mixture in solution, or perhaps in a mixture of cells, then one inhibitor capable of targeting interfaces A, B and C should be more potent than the MINK and WINK inhibitors alone, which target only interfaces A and B.

This hypothesis led to our Phase 2 inhibitors (Table 1). As shown in Fig. 4b, a Gln and Ile at positions 3 and 5 form the basis of interface C.

Table 1 | Amino acid sequences of tau inhibitors, based on two structures of the VQIINK interface.

Tau40 residue no.	274	275	276	277	278	279	280	281	282	283	
Inhibitor position	1	2	3	4	5	6	7	8	9	10	
WILD-type	K	V	Q	I	I	N	K	K	L	D	
MINK	**D**	V	Q	**M**	I	N	K	K	**R**	**K**	Phase 1
WINK	**D**	V	Q	**W**	I	N	K	K	**R**	**K**	
W-MINK	**D**	V	**W**	**M**	I	N	K	K	**R**	**K**	Phase 2
M4W39	**D**	V	**W**	M	I	N	K	K	**W**	**K**	
WMW	**D**	V	**W**	**M**	**W**	N	K	K	**R**	**K**	
WWW	**D**	V	**W**	**W**	**W**	N	K	K	**R**	**K**	

The top row lists the residue number from the native tau40 sequence. The second row lists the residue position number in the inhibitor peptide. Row 3 is the native sequence from the WT human tau40, and rows 4–9 are the inhibitor peptide sequences tested in this paper. Positions shown in bold were mutated from the WT sequence in the inhibitor peptides shown. Residues at positions 4 and 9 shown in red are critical for forming interfaces A and B, respectively. Residues 3 and 5 shown in blue comprise interface C.

Modelling indicated that substituting these positions with a tryptophan would be most destabilizing to the steric zipper structure. As summarized in Table 1, the resulting iterations of MINK incorporate a Trp steric clash at position 3, or positions 3 and 5.

As shown in Fig. 4c, the Phase 2 inhibitor W-MINK, which contains a Trp steric clash at position 3, blocked tau40 seeding more effectively than MINK, with an IC_{50} of 1.1 μM compared with 22.6 μM for MINK. Substituting the Arg at position 9 of W-MINK with a Trp (inhibitor peptide M4W39) also exhibited an improved potency over MINK, with an IC_{50} of 2.9 μM (Fig. 4f). Despite their improved IC_{50}s, the Phase 2 inhibitors still did not synergize with TLKIVW (Fig. 4d). Fluorescence images of seeded cells at two selected W-MINK concentrations, 0.3 and 2.5 μM (shown in Fig. 4e), illustrate the effect W-MINK has on seeding by tau40 fibres. At 0.3 μM W-MINK, tau40 fibres are still able to induce seeding in 4R1N tau biosensor cells, whereas at 2.5 μM W-MINK, seeding by tau40 fibres is no longer observed.

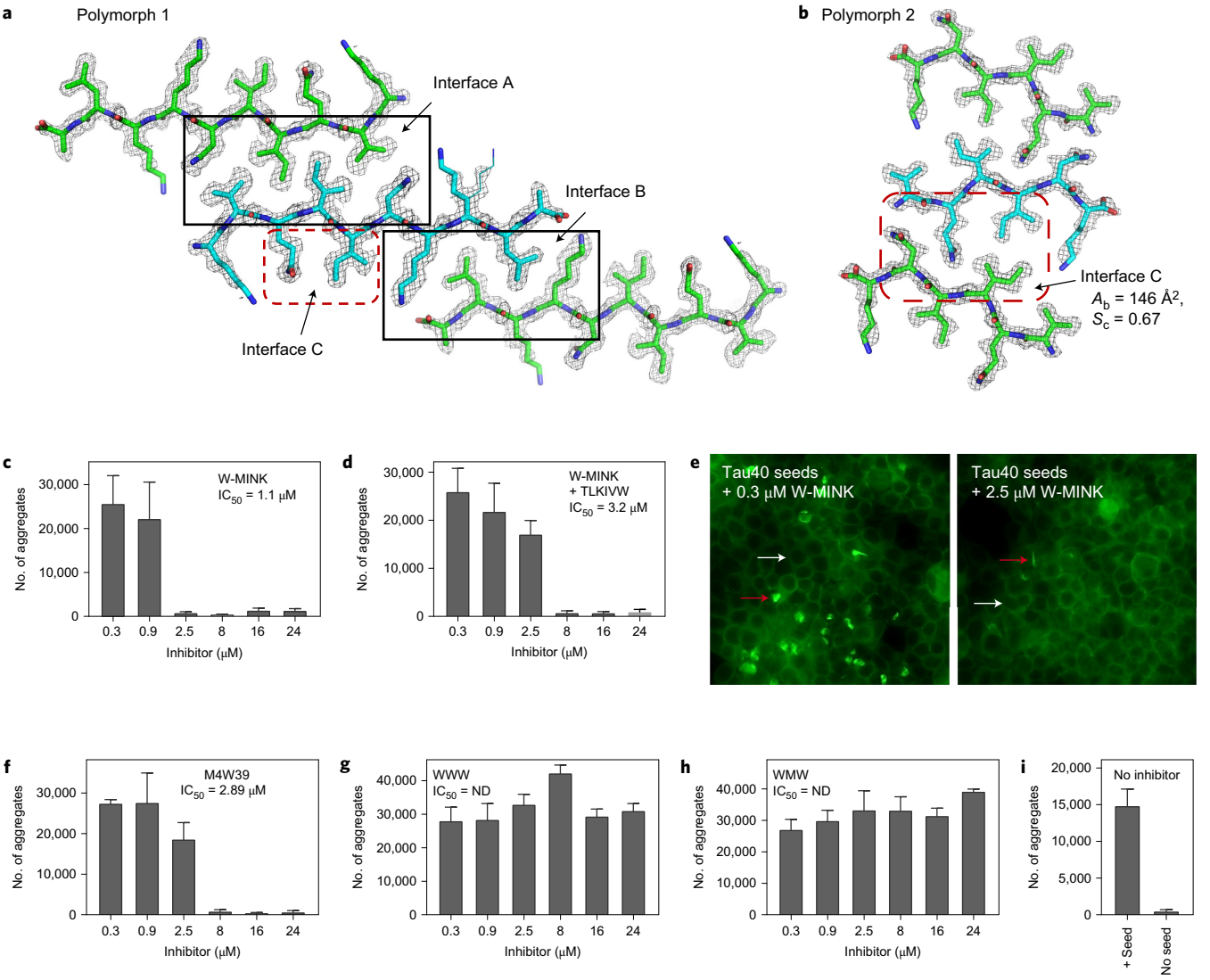

Figure 4 | The inhibition of tau aggregation by Phase 2 designed inhibitors. a,b, Comparison of the ten-residue (polymorph 1) and six-residue (polymorph 2) VQIINK MicroED structures, viewed down the fibril axes. $2F_o$–F_c electron-density maps are contoured to 1.0σ, and an alternative conformation modelled at 50% occupancy rendered in a line format is shown for Lys281 in polymorph 1. The ten-residue segment forms a face-to-face Class 1 zipper (**a**), whereas the six-residue VQIINK segment forms a face-to-back Class 4 zipper (**b**)[10]. **c**–**h**, Seeding by tau40 fibres pre-capped with Phase 2 VQIINK inhibitors (described in Table 1) designed to block interfaces A, B and C, measured in 4R1N tau-YFP biosensor cells. Bar graphs show the average number of aggregates at the indicated inhibitor concentrations, and error bars show the s.d. of triplicate measurements. The fluorescence images in **e** show seeded cells treated with 0.3 or 2.5 μM W-MINK inhibitor. Representative cells that contain aggregates are marked by red arrows, and cells without by white arrows. **i**, Quantified levels of aggregation in unseeded 4R1N tau biosensor cells, and cells seeded by untreated tau40 fibrils.

By contrast to W-MINK, the WMW peptide, which produces a Trp steric clash at both positions 3 and 5, and WWW, which contains Trp at positions 3, 4 and 5, failed to show any inhibition (Fig. 4g,h), possibly because of a destabilizing effect that multiple tryptophans in series may have on capping onto the amyloid chain. These data suggest that the Ile at position 5 in interface C is insensitive to substitution, whereas the Gln at position 3 (Gln 276 in the native sequence) plays an important role in stabilizing interface C.

Discussion

Prior to the two atomic structures of the VQIINK segment reported here, the atomic-level understanding of how R2 contributes to tau aggregation was limited. The crystals of tau that included the VQIINK segment were invariably some 10,000 times smaller in volume than crystals of the other fibril-driving segment VQIVYK, and thus too tiny for manipulation and X-ray data collection. Electron diffraction came to the rescue, as it provides atomic-resolution structures of fibrils of both the ten-residue amyloid-forming segment with sequence KVQIINKKLD and the six-residue structure of VQIINK itself.

Both structures reveal a propensity of VQIINK to form tightly interdigitated steric-zipper interfaces that appear to be more adhesive than the interface of VQIVYK. Biochemical studies support this interpretation as they showed that engineered tau constructs that contain only VQIINK aggregate more rapidly than WT, and constructs that contain only VQIVYK instead accrue a mixture of monomer, oligomer and fibre. These data indicate that VQIINK is a potent driver of tau amyloid aggregation, and that it is probably an excellent target for the inhibitors of full-length tau fibril formation.

Our VQIINK structures explain observations that have been made previously. The structure of the ten-residue segment shows that Ile277 projects into interface A to form the centrepiece for the aggregation of this motif. Previous studies highlighted the importance of Ile277 by showing that I277P disrupts the tau amyloid fibre structure[19]. Additionally, as described in Fig. 1d, our structure provides insight into how the deletion of Lys280 can enhance tau fibril formation by extending interface A, which nearly doubles the contiguous buried surface area of the steric zipper interface for the ΔK280 mutant.

These two VQIINK-containing structures enabled the design of VQIINK inhibitors that act on full-length tau by capping the ends of tau fibrils to prevent template-assisted filament growth[11,24]. The VQIINK inhibitors tested here slow full-length tau aggregation *in vitro* and, furthermore, block seeding induced by tau40 fibres in 4R1N tau HEK293 biosensor cells. This is significant because, as we show, VQIVYK inhibitors were unable to inhibit seeding by tau40. The failure of VQIVYK inhibitors to block seeding might be viewed as conflicting with the observation that VQIVYK is central to the core of tau fibrils extracted from AD tissue[25]. As we discuss in the following paragraph, however, our findings may be consistent with this observation.

Tau fibrils extracted from the AD brain adopt a fibril core that comprises R3 and repeat 4 (R4), in addition to ten residues that extend beyond the end of R4. VQIINK and the rest of R2 apparently reside in the fuzzy coat of this AD fibril. This seems to suggest that VQIVYK-capping inhibitors should be highly effective at blocking seeding by tau40 fibres. To the contrary, our results show that VQIINK is the more prominent effector of seeding by tau40, at least for recombinant fibrils. How can these two observations be reconciled? One possibility is that the core of the tau fibril formed *in vitro* differs from that found in AD. Alternatively, it is possible that the fibril core itself is not the primary driver of seeding, but rather serves as a solvent-excluded scaffold that clusters VQIINK segments together in the fuzzy coat, and thereby poises the solvent-exposed VQIINK steric zippers for seeding. From this perspective, VQIINK localization to the fuzzy coat would make it more accessible to protein monomers in the cellular milieu, which in turn explains its prominent role in seeding and its exquisite sensitivity to inhibition. Interpreted this way, our VQIINK structures are consistent with the AD-derived tau fibril model reported by Fitzpatrick *et al.* (2017).

Our studies emphasize that the effectiveness of inhibitor treatment depends on the stage of administration of the inhibitor. That is, the concentration of inhibitor required to block seeding by pre-formed fibres is about 100 times greater than the amount required when the inhibitor is added to monomeric tau prior to initiating aggregation by shaking and the addition of heparin, when 250 nM inhibitor effectively inhibited seeding. The greater amount of inhibitor required to block pre-formed fibres probably stems from the propensity of mature fibres to extend unabated to produce longer fibres with more surface area for seeding by secondary nucleation and/or fragmentation into smaller species that produce new sites for primary nucleation. This observation may highlight the importance of early disease intervention with amyloid inhibitors, which underlines the need for sensitive disease biomarkers.

Our structures of VQIINK may suggest a structural basis for the mysterious phenomenon of tau strains[22,26]. Whereas strains in microorganisms are different phenotypes encoded by different nucleic acid sequences, strains in amyloid diseases are different phenotypes encoded by different fibril structures. Different fibril structures, in turn, are probably encoded by the formation of different steric zippers[27]. Three distinctly different steric zippers emerged from our two VQIINK structures: interfaces A, B and C. The existence of these distinct interfaces shows how conformationally distinct fibrils of tau can form, and we speculate that these different structures may begin to reveal how a subset of different tau strains could originate at the molecular level, although future studies will be needed to address this possibility directly.

Methods

Crystallization, data collection and structure solution. Nanocrystals of KVQIINKKLD synthetic peptide (purchased from Genscript) were prepared from 30 mg ml^{-1} stocks dissolved in water by the addition of 45 mM arachidonic acid to concentrated peptide. Subsequently, crystals were grown in batch at 37 °C by the addition of 10 µl of precipitant (32% PEG10K in 100 mM phosphate citrate, pH 4.2) to 5 µl of protein. After 18 h, nanocrystals were resuspended by pipetting, spun down in an epitube and the resulting crystalline pellet was washed three times with water. Nanocrystals of the VQIINK peptide (purchased from Genscript) were grown by vapour diffusion from the peptide at 15 mg ml^{-1} as a 1:2 drop ratio (protein: reservoir) from 0.29 M $LiNO_3$, 24% (w/v) PEG 3350 at 18 °C and similarly harvested for data collection.

MicroED data were collected by spotting 2–3 µl of crystals onto transition electron microscope (TEM) grids with a carbon film support and plunge frozen in liquid ethane using a Vitrobot Mark IV (FEI). Diffraction images were collected on an FEI Tecnai F20 TEM at 200 kV as a continuous rotation tilt series at a rate of 0.2° per second with two seconds of exposures per image. Diffraction data from several crystals were indexed, merged and scaled with XDS and XSCALE[28]. Molecular replacement was performed with Phaser[29] using a polyalanine search model composed of an ideal β-strand. The structure of VQIINK was solved using a truncated version of KVQIINKKLD that comprised residues 2–7 (VQIINK) as a search model in Phaser. Crystallographic refinements were performed using the programs Refmac[30], Buster[31] and Coot[32].

Inhibitor peptide design. VQIINK inhibitor peptides were designed using the native structure as a starting point. Bulky side chains were modelled at sites in the VQIINK structure that were in close contact with residues in the mated sheet of the steric zipper interface, as shown in Fig. 3a. Capping residues were chosen by modelling all the possible rotamers to find side chains without any compatible conformer with the steric zipper interface (that is, side chains that clashed with the mated β-sheet at every rotamer conformer were selected). All the inhibitor peptides shown in Table 1 were synthesized by Genscript with minimum purities of 90% and dissolved in deionized water to a final stock concentration of 6 mM.

Tau fibril incubation with inhibitors for biosensor cell-seeding assays. Tau40 fibres were prepared by shaking 25 µM tau40 in PBS buffer (pH 7.4) with 0.5 mg ml^{-1} heparin (Sigma cat. no. H3393) and 1 mM dithiothreitol (DTT) for 3–6 days. The presence of fibres was confirmed with an endpoint ThT reading, and then fibrils

were diluted 20-fold to 1.25 μM in OptiMEM (Life Technologies, cat. no. 31985070). Inhibitors dissolved in water were added to 20 μl of diluted tau40 fibres at a concentration 20-fold greater than the final desired concentration. For combination VQIINK inhibitor treatments with TLKIVW, the indicated concentration is the total amount of inhibitor, which is the sum of each individual inhibitor present at an equimolar ratio. The D-TLKIVW peptide was first dissolved to a high concentration in DMSO (>25 mM), and then diluted in water before addition to the fibres. The fibres were incubated for 16 h with the inhibitor, and subsequently were sonicated in a Cup Horn water bath for 3 min before seeding the cells. The resulting 'pre-capped fibrils' were mixed with one volume of Lipofectamine 2000 (Life Technologies, cat. no. 11668027) prepared by diluting 1 μl of Lipofectamine in 19 μl of OptiMEM. After 20 min, 10 μl of fibrils were added to 90 μl of the 4R1N tau biosensor cells to achieve the final indicated ligand concentration.

ThT plate-reader assay. Concentrated tau protein was diluted into PBS buffer (pH 7.4) to a final concentration, as indicated in the text. Proteins were shaken as solutions that contained 75 μM ThT, 0.5 mg ml^{-1} heparin (Sigma cat. no. H3393), 1 mM DTT and a twofold molar excess of inhibitor (when indicated) in 96-well plates with a plastic bead to enhance agitation. ThT fluorescence was measured with excitation and emission wavelengths of 440 and 480 nm, respectively, and averaged curves were generated from triplicate measurements, as indicated in the figure legend. Error bars show the s.d. of replicate measurements.

Life Sciences Reporting Summary. Further information on experimental design and reagents is available in the Life Sciences Reporting Summary.

Data availability. Atomic coordinates and structure factors have been deposited in the Protein Data Bank (PDB) under accession codes 5V5B (KVQIINKKLD) and 5K7N (VQIINK).

Received 22 February 2017; accepted 4 October 2017; published online 20 November 2017

References

1. Margittai, M. & Langen, R. Side chain-dependent stacking modulates tau filament structure. *J. Biol. Chem.* **281,** 37820–37827 (2006).
2. von Bergen, M. *et al.* Assembly of τ protein into Alzheimer paired helical filaments depends on a local sequence motif (306VQIVYK311) forming β structure. *Proc. Natl Acad. Sci. USA* **97,** 5129–5134 (2000).
3. Goedert, M., Eisenberg, D. S. & Crowther, R. A. Propagation of tau aggregates and neurodegeneration. *Annu. Rev. Neurosci.* **40,** 189–210 (2017).
4. Schwarz, A. J. *et al.* Regional profiles of the candidate tau PET ligand recapitulate key features of Braak histopathological stages. *Brain* **139,** 1539–1550 (2016).
5. Manczak, M. & Reddy, P. H. Abnormal interaction of oligomeric amyloid-β with phosphorylated tau: implications to synaptic dysfunction and neuronal damage. *J. Alzheimers Dis.* **36,** 285–295 (2013).
6. Seward, M. E. *et al.* Amyloid-β signals through tau to drive ectopic neuronal cell cycle re-entry in Alzheimer's disease. *J. Cell Sci.* **126,** 1278–1286 (2013).
7. Brier, M. R. *et al.* Tau and Aβ imaging, CSF measures, and cognition in Alzheimer's disease. *Sci. Transl. Med.* **8,** 338ra366 (2016).
8. Kfoury, N., Holmes, B. B., Jiang, H., Holtzman, D. M. & Diamond, M. I. Trans-cellular propagation of tau aggregation by fibrillar species. *J. Biol. Chem.* **287,** 19440–19451 (2012).
9. von Bergen, M. *et al.* Mutations of tau protein in frontotemporal dementia promote aggregation of paired helical filaments by enhancing local beta-structure. *J. Biol. Chem.*, **276,** 48165–48174 (2001).
10. Sawaya, M. R. *et al.* Atomic structures of amyloid cross-[bgr] spines reveal varied steric zippers. *Nature* **447,** 453–457 (2007).
11. Sievers, S. A. *et al.* Structure-based design of non-natural amino-acid inhibitors of amyloid fibril formation. *Nature* **475,** 96–100 (2011).
12. Zheng, J. *et al.* Macrocyclic β-sheet peptides that inhibit the aggregation of a tau-protein-derived hexapeptide. *J. Am. Chem. Soc.* **133,** 3144–3157 (2011).
13. Shi, D., Nannenga, B. L., Iadanza, M. G. & Gonen, T. Three-dimensional electron crystallography of protein microcrystals. *eLife* **2,** e01345 (2013).
14. Rodriguez, J. A. *et al.* Structure of the toxic core of [agr]-synuclein from invisible crystals. *Nature* **525,** 486–490 (2015).
15. Rodriguez, J. A. & Gonen, T. in *Methods in Enzymology* Vol. 579 (ed. Crowther, R. A.) 369–392 (Academic, 2016).
16. Eisenberg, D. S. & Sawaya, M. R. Structural studies of amyloid proteins at the molecular level. *Annu. Rev. Biochem.* **86,** 3.1–3.27 (2017).
17. Wood, S. J., Wetzel, R., Martin, J. D. & Hurle, M. R. Prolines and amyloidogenicity in fragments of the Alzheimer's peptide β/A4. *Biochemistry* **34,** 724–730 (1995).
18. Moore, C. L. *et al.* Secondary nucleating sequences affect kinetics and thermodynamics of tau aggregation. *Biochemistry* **50,** 10876–10886 (2011).
19. von Bergen, M. *et al.* Mutations of tau protein in frontotemporal dementia promote aggregation of paired helical filaments by enhancing local β-structure. *J. Biol. Chem.* **276,** 48165–48174 (2001).
20. Margittai, M. & Langen, R. Fibrils with parallel in-register structure constitute a major class of amyloid fibrils: molecular insights from electron paramagnetic resonance spectroscopy. *Q. Rev. Biophys.* **41,** 265–297 (2008).
21. Mirbaha, H., Holmes, B. B., Sanders, D. W., Bieschke, J. & Diamond, M. I. Tau trimers are the minimal propagation unit spontaneously internalized to seed intracellular aggregation. *J. Biol. Chem.*, **290** 14893–14903 (2015).
22. Sanders, D. W. *et al.* Distinct tau prion strains propagate in cells and mice and define different tauopathies. *Neuron* **82,** 1271–1288 (2014).
23. Siddiqua, A. *et al.* Conformational basis for asymmetric seeding barrier in filaments of three- and four-repeat tau. *J. Am. Chem. Soc.* **134,** 10271–10278 (2012).
24. Margittai, M. & Langen, R. Template-assisted filament growth by parallel stacking of tau. *Proc. Natl Acad. Sci. USA* **101,** 10278–10283 (2004).
25. Fitzpatrick, A. W. P. *et al.* Cryo-EM structures of tau filaments from Alzheimer's disease. *Nature* **547,** 185–190 (2017).
26. Kaufman, S. K. *et al.* Tau prion strains dictate patterns of cell pathology, progression rate, and regional vulnerability *in vivo*. *Neuron* **92,** 796–812 (2016).
27. Wiltzius, J. J. W. *et al.* Molecular mechanisms for protein-encoded inheritance. *Nat. Struct. Mol. Biol.* **16,** 973–978 (2009).
28. Kabsch, W. XDS. *Acta Crystallogr. D* **66,** 125–132 (2010).
29. McCoy, A. J. *et al.* Phaser crystallographic software. *J. Appl. Crystallogr.* **40,** 658–674 (2007).
30. Murshudov, G. N., Vagin, A. A. & Dodson, E. J. Refinement of macromolecular structures by the maximum-likelihood method. *Acta Crystallogr. D* **53,** 240–255 (1997).
31. Bricogne, G., B. E. *et al. BUSTER 2.10.0* (Global Phasing Ltd, 2016).
32. Emsley, P., Lohkamp, B., Scott, W. G. & Cowtan, K. Features and development of Coot. *Acta Crystallogr D* **66,** 486–501 (2010).

Acknowledgements

We thank M. Diamond for discussion and for gifting the monoclonal biosensor HEK293 cell-line that expressed tau 4R1N P301S-EYFP for our inhibitor assay, and H. Mirbaha for assistance and advice on conducting the biosensor seeding experiments and purifying K18 tau oligomers by gel filtration chromatography. We also thank awards 1R01 AG029430 and RF1 AG054022 from the National Institute on Aging, 1F32 NS095661 from the National Institute of Neurological Disorders and Stroke, A2016588F from the BrightFocus Foundation and HHMI and the Janelia Visiting Scientist Program for support.

Author contributions

P.M.S. conceived and designed the experiments; P.M.S., D.R.B., J.A.R. and K.M. performed the experiments; P.M.S., D.R.B., M.R.S. and D.C. analysed data; and P.M.S., D.S.E. and T.G. co-wrote the paper.

Additional information

Supplementary information is available in the online version of the paper. Reprints and permissions information is available online at www.nature.com/reprints. Publisher's note: Springer Nature remains neutral with regard to jurisdictional claims in published maps and institutional affiliations. Correspondence and requests for materials should be addressed to D.S.E.

Competing financial interests

D.S.E. is chair of the scientific advisory board of ADRx.

nature research

Corresponding Author: David Eisenberg

Date: Sep 22, 2017

Life Sciences Reporting Summary

Nature Research wishes to improve the reproducibility of the work we publish. This form is published with all life science papers and is intended to promote consistency and transparency in reporting. All life sciences submissions use this form; while some list items might not apply to an individual manuscript, all fields must be completed for clarity.

For further information on the points included in this form, see Reporting Life Sciences Research. For further information on Nature Research policies, including our data availability policy, see Authors & Referees and the Editorial Policy Checklist.

Experimental design

1. Sample size

   Describe how sample size was determined. — All experiments were performed with three replicates

2. Data exclusions

   Describe any data exclusions. — No data was excluded

3. Replication

   Describe whether the experimental findings were reliably reproduced. — All experiments were reproduced a minimum of two times

4. Randomization

   Describe how samples/organisms/participants were allocated into experimental groups. — Samples were grouped by concentration, and covariates were controlled for by assigning each sample a letter code which was used to identify the samples composition after data collection was completed.

5. Blinding

   Describe whether the investigators were blinded to group allocation during data collection and/or analysis. — Blinding was carried out as described in 4. Samples were assigned a letter code that was used to identify the samples composition after data collection was completed.

Note: all studies involving animals and/or human research participants must disclose whether blinding and randomization were used.

6. Statistical parameters

   For all figures and tables that use statistical methods, confirm that the following items are present in relevant figure legends (or the Methods section if additional space is needed).

n/a	Confirmed	
☐	☒	The exact sample size (*n*) for each experimental group/condition, given as a discrete number and unit of measurement (animals, litters, cultures, etc.)
☐	☒	A description of how samples were collected, noting whether measurements were taken from distinct samples or whether the same sample was measured repeatedly.
☐	☒	A statement indicating how many times each experiment was replicated
☒	☐	The statistical test(s) used and whether they are one- or two-sided (note: only common tests should be described solely by name; more complex techniques should be described in the Methods section)
☒	☐	A description of any assumptions or corrections, such as an adjustment for multiple comparisons
☒	☐	The test results (e.g. *p* values) given as exact values whenever possible and with confidence intervals noted
☐	☒	A summary of the descriptive statistics, including central tendency (e.g. median, mean) and variation (e.g. standard deviation, interquartile range)
☐	☒	Clearly defined error bars

See the web collection on statistics for biologists for further resources and guidance.

Software

Policy information about availability of computer code

7. Software

Describe the software used to analyze the data in this study.	Graphs were plotted in Excel and analyzed using GraphPad Prism. Diffraction data was indexed, merged and scaled with XDS and XSCALE. Molecular replacement was performed with Phaser, and refinements were performed using Refmac, Buster, and Coot

For all studies, we encourage code deposition in a community repository (e.g. GitHub). Authors must make computer code available to editors and reviewers upon request. The *Nature Methods* guidance for providing algorithms and software for publication may be useful for any submission.

Materials and reagents

Policy information about availability of materials

8. Materials availability

Indicate whether there are restrictions on availability of unique materials or if these materials are only available for distribution by a for-profit company.	There is no restriction on the availability of materials used in this study

9. Antibodies

Describe the antibodies used and how they were validated for use in the system under study (i.e. assay and species).	No antibodies were used in this study

10. Eukaryotic cell lines

a. State the source of each eukaryotic cell line used.	HEK293 cell lines stably expressing Tau 4R1N P301S-EYFP , referred to as "4R1N Tau biosensor cells" were engineered by Marc Diamond's lab at UTSW.
b. Describe the method of cell line authentication used.	None of the cell lines used were authenticated by us
c. Report whether the cell lines were tested for mycoplasma contamination.	None of the cell lines used were tested for mycoplasma contamination by us
d. If any of the cell lines used in the paper are listed in the database of commonly misidentified cell lines maintained by ICLAC, provide a scientific rationale for their use.	No commonly misidentified cell lines were used

Animals and human research participants

Policy information about studies involving animals; when reporting animal research, follow the ARRIVE guidelines

11. Description of research animals

Provide details on animals and/or animal-derived materials used in the study.	no animals were used

Policy information about studies involving human research participants

12. Description of human research participants

Describe the covariate-relevant population characteristics of the human research participants.	the study did not involve human participants